

Supporting Information

The Assembly of Multifunctional Ni₂P/NiS_{0.66} Heterostructures and Their Superstructure for High Lithium and Sodium Anodic Performance

Tian Wu^{a, b}, Sanpei Zhang^{a, b}, Qiming He^{a, b}, Xiaoheng Hong^{a, b}, Fan Wang^{a, b},

*Xiangwei Wu^a, Jianhua Yang^a and Zhaoyin Wen^{a, *}*

^a *CAS key laboratory of Materials for Energy Conversion, Shanghai Institute of Ceramics, Chinese Academy of Sciences, Shanghai 200050, P.R. China*

^b *University of Chinese Academy of Sciences, Beijing, 100039, P.R. China*

*E-mail: zywen@mail.sic.ac.cn

Experimental section

Materials. All reagents in this work were used directly without any further purification. Nickel nitrate hexahydrate ($\text{Ni}(\text{NO}_3)_2 \cdot 6\text{H}_2\text{O}$, 99.9%, Aladdin), ethanol (98%, Aladdin) trimesic acid (99% Aladdin), N,N-dimethylformamide (DMF, Aladdin), Polyvinyl pyrrolidone (PVP, 98%, $M_w = 58000$), N-methyl-2-pyrrolidone (NMP, Sigma-Aldrich 99.9%), lithium hexafluorophosphate (LiPF_6 , Battery grade, Aladdin), ethylene carbonate (EC, 99.9% Sigma-Aldrich), dimethyl carbonate (DMC, 99% Sigma-Aldrich), fluoroethylene carbonate (FEC, 98% Sigma-Aldrich), sodium perchlorate (NaClO_4 , 98% Sigma-Aldrich), sodium (99.8% Aladdin), and lithium foil (12 mm in diameter) were used as received. Commercial $\text{LiNi}_{1/3}\text{Co}_{1/3}\text{Mn}_{1/3}\text{O}_2$ (LNCMO) electrode materials came from CITIC Guoan mengguli Power Technology Co., Ltd. (China).

Synthesis of Ni-precursors. In a typical synthesis process, 432 mg of $\text{Ni}(\text{NO}_3)_2 \cdot 6\text{H}_2\text{O}$, 750 mg PVP and 150 mg trimesic acid (H_3BTC) were dissolved in 15 mL deionized water and sonicated for 30 min. Then the obtained light green solution was added into a mixture solution (15 mL of ethanol and 15 mL of DMF) under 30 min vigorous stirring to form a uniform solution. The mixed solution was transferred into a 50 mL Teflon-lined stainless-steel autoclave and heated to 150 °C for 8h. The green products were collected by centrifugation at 8000 rpm, and washed with ethanol for three times and dried in an oven overnight at 65 °C.

Synthesis of HT-NPS@C nanospheres. The HT-NPS@C nanospheres were fabricated by a two-step thermal treatment method. In order to obtain the NP@C nanospheres, the as-synthesized green Ni-precursors (50 mg) and $\text{NaH}_2\text{PO}_2 \cdot \text{H}_2\text{O}$ (100 mg) were placed at two separate positions in a quartz boat with $\text{NaH}_2\text{PO}_2 \cdot \text{H}_2\text{O}$ at the upstream side. Finally, the samples were heated to 450 °C for 2 h with a ramp of 3 °C/min under N_2 gas flow. The HT-NPS@C nanospheres were synthesized through a similar sulfidation process. Thiourea powder (99.8% Aladdin) was put on the upstream side of the boat. The resulting powders were again heated to 450 °C for 2 h

in N₂ gas with a ramp of 3 °C/min. The as-prepared HT-NPS@C nanospheres were washed with deionized water and dried at 50 °C in vacuum.

Material Characterization: X-ray powder diffraction (XRD) analysis of the as-obtained samples was carried out with a Rigaku Ultima IV with Cu-K α radiation ($\lambda = 1.5418 \text{ \AA}$), operated at 40 kV and 20 mA. The morphology of the samples was observed using SEM (S-4800N, Hitachi), FESEM (SU-8200, Hitachi) and TEM (JEM-2100F) equipped with an EMSA/MAS energy dispersive spectroscopy (EDS). The chemical composition of the samples was analyzed by XPS (Kratos AXIS ULTRA X-ray photoelectron microscope with Al-K α X-rays as the excitation source) The core level energies were calibrated with the C 1s binding energy of 284.8 eV. The carbon content in HT-NPS@C was detected using thermogravimetric analyzer (Netzsch STA 409PC) under air atmosphere from room temperature to 810 °C at a heating rate of 5 °C min⁻¹.

Battery assembly. Electrochemical measurements were performed using CR2025 coin-type cells assembled in an Ar-filled glove box with oxygen and water contents less than 0.1 ppm. For the LIBs, lithium foil and glass fiber (Whatman) are used as counter electrode and separator, respectively. The electrolyte is 1 M LiPF₆ in ethylene carbonate (EC), dimethyl carbonate (DMC) (1:1 v/v), and 5 wt% fluoride ethylene carbonate (FEC). For the SIBs, sodium and glass fiber membrane are used as counter electrode and separator, respectively. The electrolyte involves 1 M sodium perchlorate in EC and DMC (1:1 v/v) solution with 10 wt % FEC. The working electrode slurry was prepared by mixing 80% active material, 10% Super P, and 10% PVDF with NMP. Then, the slurry was uniformly cast on the copper foil current collector and dried in vacuum oven at 80 °C for 24 hours. The diameter of working electrodes is 12 mm. The average mass loading of the active material on each electrode is 1.0 ~ 2.0 mg cm⁻². All the capacity values of HT-NPS@C and NP@C are calculated based on the mass of Ni₂P nanocrystals.

Full cell lithium ion battery assembly. The CR2025 coin-type full-cells were assembled by using HT-NPS@C anodes and LNCMO cathodes with a mass loading of about 1.3 mg cm^{-2} and 4.8 mg cm^{-2} , respectively. The HT-NPS@C anodes were pre-lithiated/delithiated to the irreversible capacity loss in the first cycle. The LNCMO electrode slurry was prepared by mixing 80% LNCMO, 10% Super P, and 10% PVDF with NMP. The slurry was uniformly cast on the alumina foil current collector and dried in vacuum oven at $80 \text{ }^{\circ}\text{C}$ for 24 hours. The diameter of working electrodes is 12 mm. Before assembling the full cells, the HT-NPS@C anodes were pre-lithiated/delithiated to decrease the irreversible capacity loss in the first cycle.

1. SEM and TEM images of Ni-precursor.

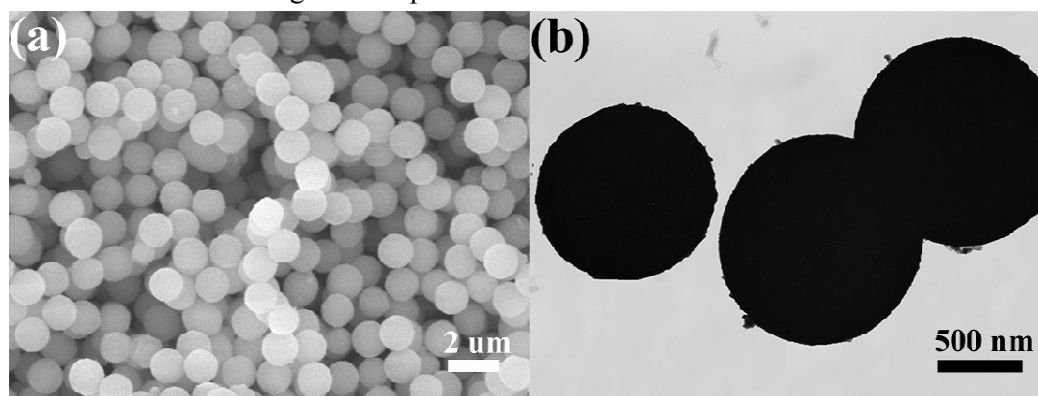


Figure. S1. (a)SEM image and (b)TEM image for the Ni-precursor.

2. . XRD pattern of the Ni-precursor.

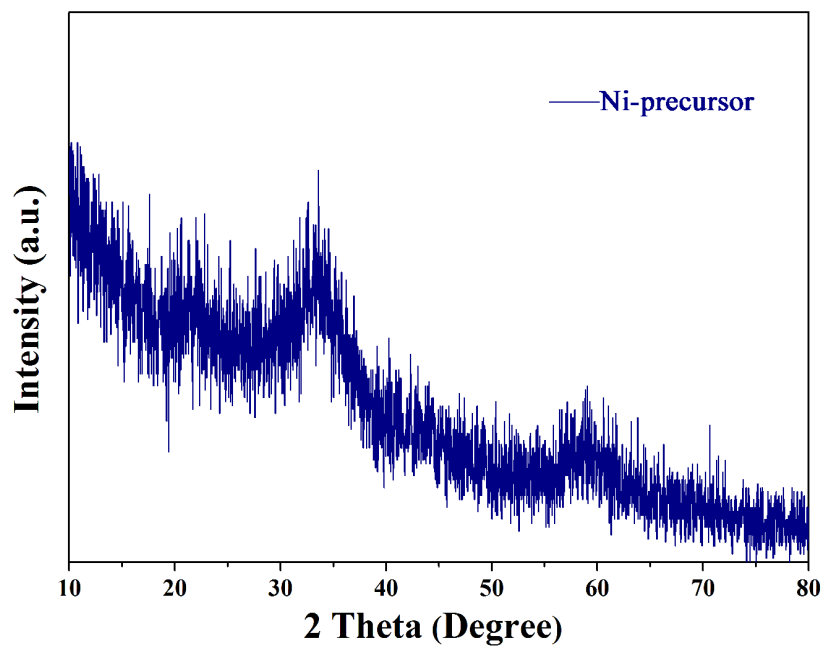


Figure. S2. XRD pattern of the Ni-precursor.

3. Elemental mapping images of the NP@C nanospheres.

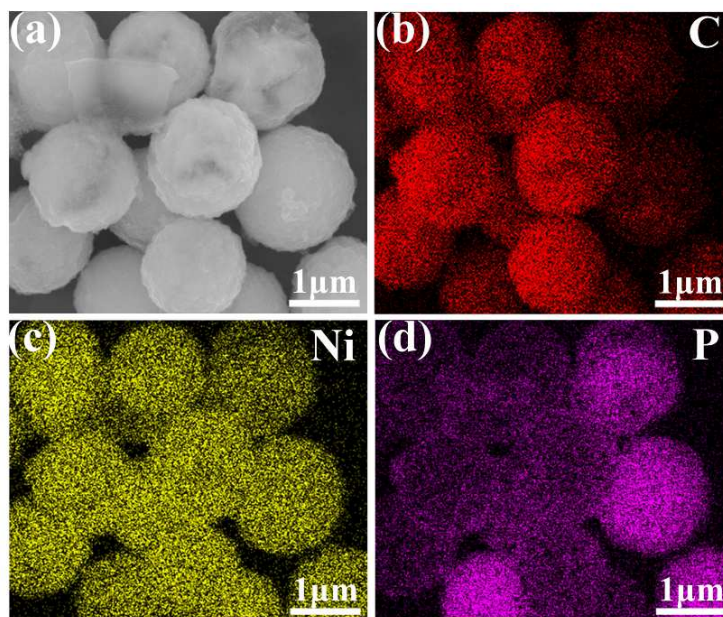


Figure. S3. The SEM image (a) and corresponding elemental mapping images (b-d) of the NP@C nanospheres.

4. XRD pattern of the NP@C microspheres.

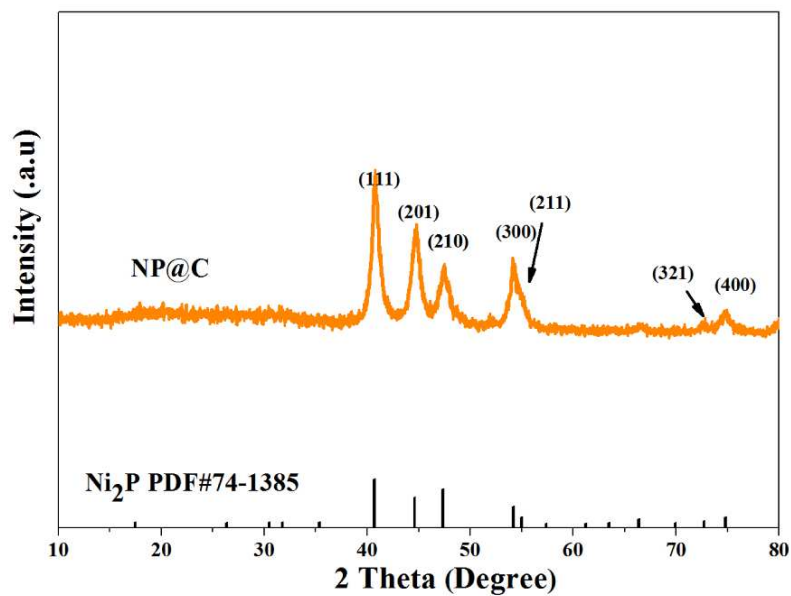


Figure. S4. XRD pattern of the NP@C microspheres.

5. TGA and DSC curves of HT-NPS@C.

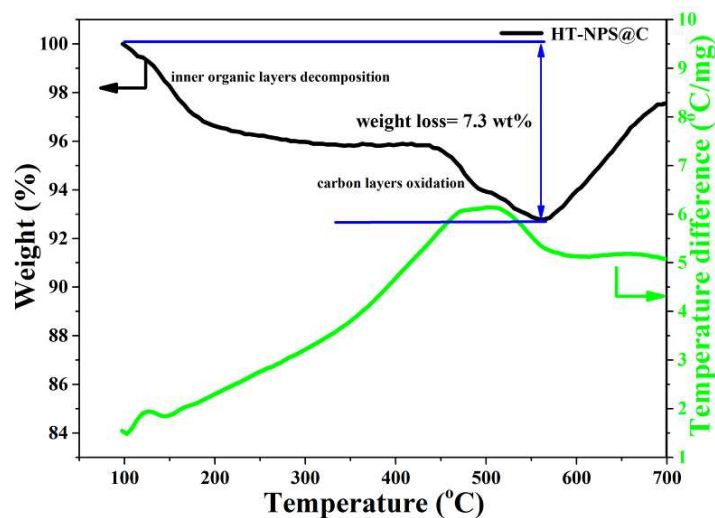


Figure. S5. TGA curves of HT-NPS@C. There are no obvious reactions below 300 °C according to the corresponding DSC curve. The weight loss of the whole system results from the evaporation and decomposition of the inner organic layers. It is considered that the further decrease in weight when heated above 400 °C was probably due to oxidation of carbon layers of HT-NPS@C in air. The whole weight increased again after 580 °C, indicating that some obvious reactions occurred. (Ni_2P transforms to Ni_2POx) Therefore, the carbon and Ni_2P content of HT-NPS@C are measured to be 3.3%, 92.7%, respectively.

6. EDX analysis of HT-NPS@C.

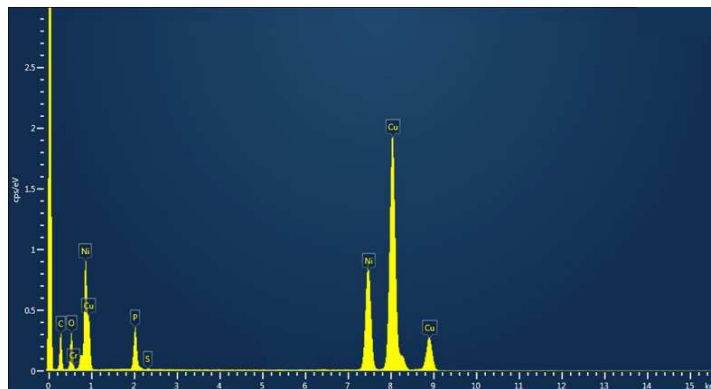


Figure. S6. EDX spectra of HT-NPS@C. From Fig.S4, the main elements of the HT-NPS@C nanospheres are clearly detected by EDS. Besides Ni, P, C and S, oxygen associated with metal oxide and phosphorus oxide is also detected. It is ascribed to passivation that occurs when HT-NPS@C is exposed to air.

7. XPS and EDX results of atomic content of various elements in the as-prepared HT-NPS@C

Table S1. Atomic content of various elements in the as-prepared HT-NPS@C.

	Ni (%)	P (%)	C (%)	S (%)
XPS	48.22	23.99	24.97	2.82
EDX	52.68	23.79	21.19	2.34
Average	50.45	23.89	23.08	2.58

8. XPS survey spectra of HT-NPS@C and NP@C.

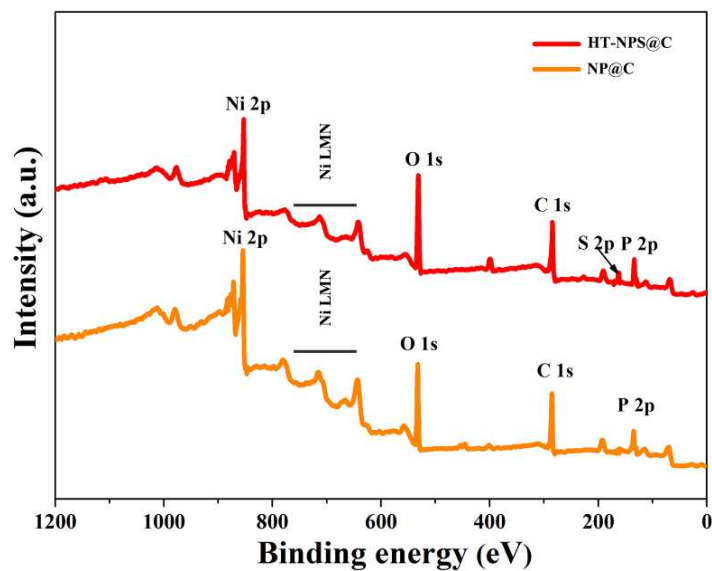


Figure. S7. XPS survey spectrum of HT-NPS@C and NP@C.

9. High resolution C 1s spectra of NP@C and HT-NPS@C.

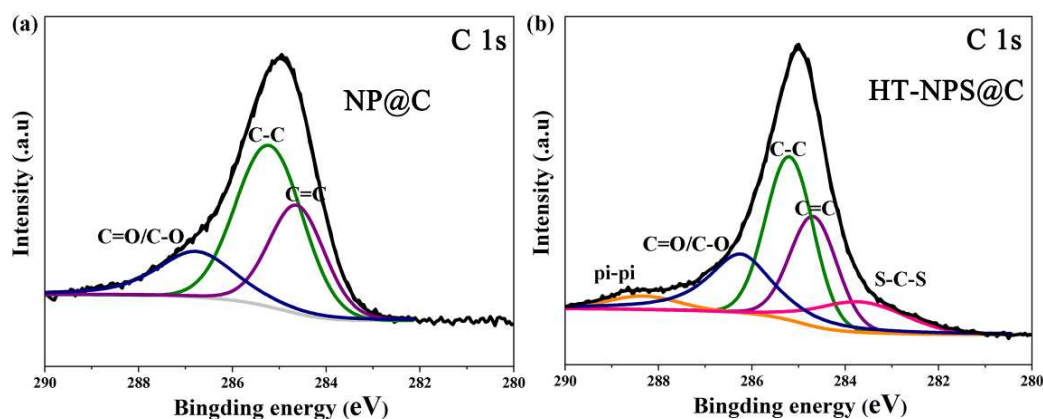


Figure. S8. High resolution C 1s spectra of NP@C (a) and HT-NPS@C (b). From Fig.S5, the changes in NP@C and HT-NPS@C were observed more clearly in the high-resolution C 1s. These peaks correspond to C=C (284.5 eV), C-C (285.4 eV, 33.83), C-S-C (283.9 eV), C-O/C=O (286.6 eV), and pi-pi (288.9 eV).

10. The initial five discharge and charge curves of the NP@C electrode.

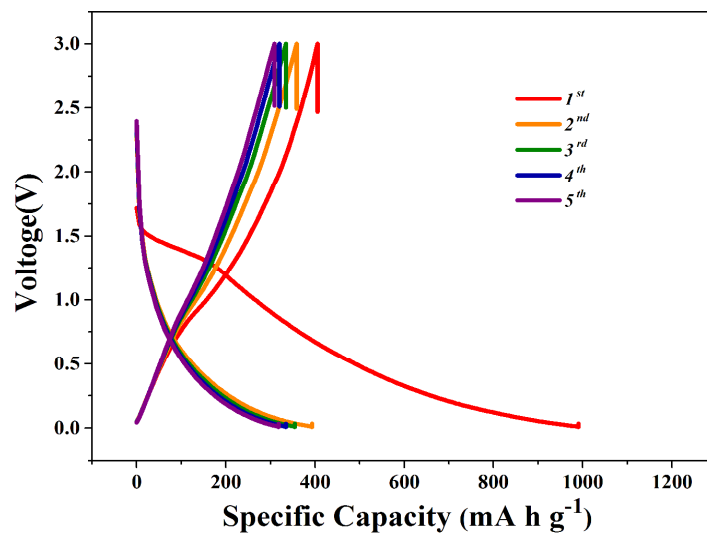


Figure. S9. Initial charge/discharge profiles of the NP@C electrode at 0.1 A g⁻¹. The first-cycle discharge and charge capacities are 998.6 and 405.2 mA h g⁻¹, respectively. The discharge process of the LIBs based on NP@C and HT-NPS electrodes is mainly carried out below 1.5 V, which makes it a promising anode material.

11. Impedance spectra of the HT-NPS@C and NP@C electrodes after five cycles cycling.

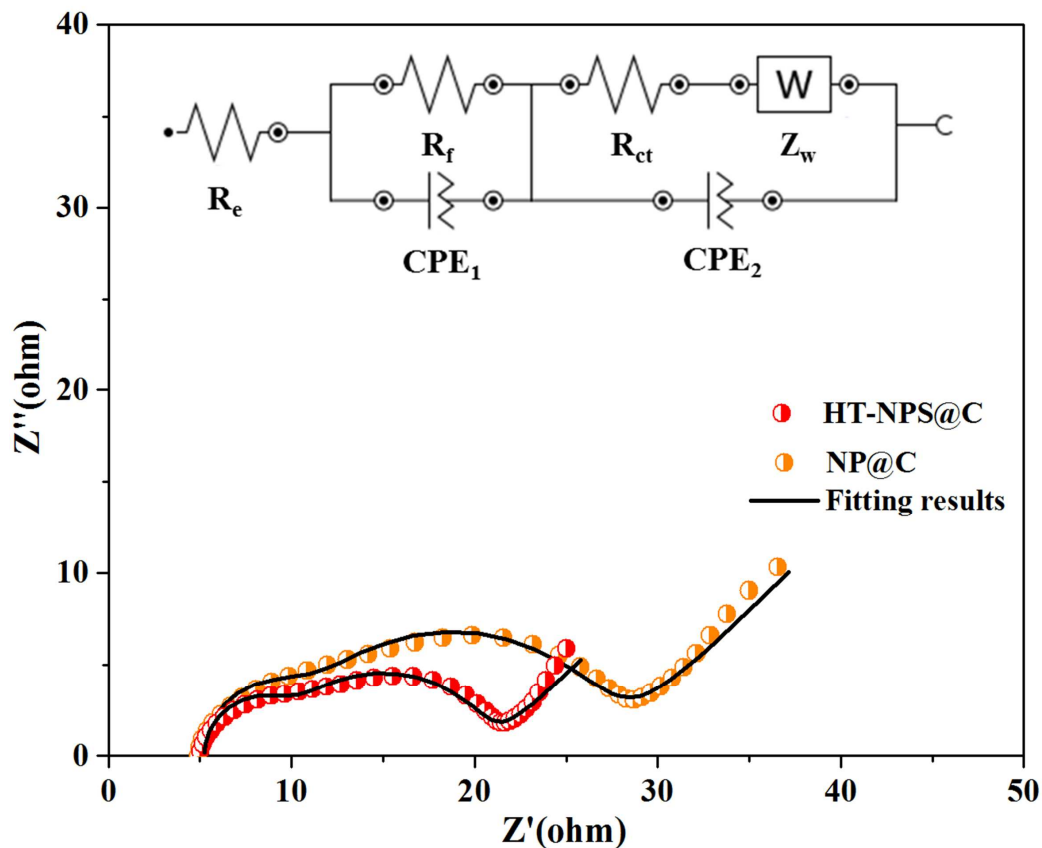


Figure. S10. Impedance spectra of the HT-NPS@C and NP@C electrodes after five cycles cycling (fully lithiated). The inset is the equivalent circuit. R_e represents the impedance contributed by the electrolyte; R_f and CPE_1 represent the resistance and capacitance of the SEI films, respectively (high-frequency). R_{ct} and CPE_2 are the charge-transfer resistance and the double-layer capacitance, respectively (medium-frequency). Z_w is the Warburg impedance related to the diffusion of lithium ions into the bulk electrodes.

12. The initial five discharge and charge curves of the LNCMO electrode.

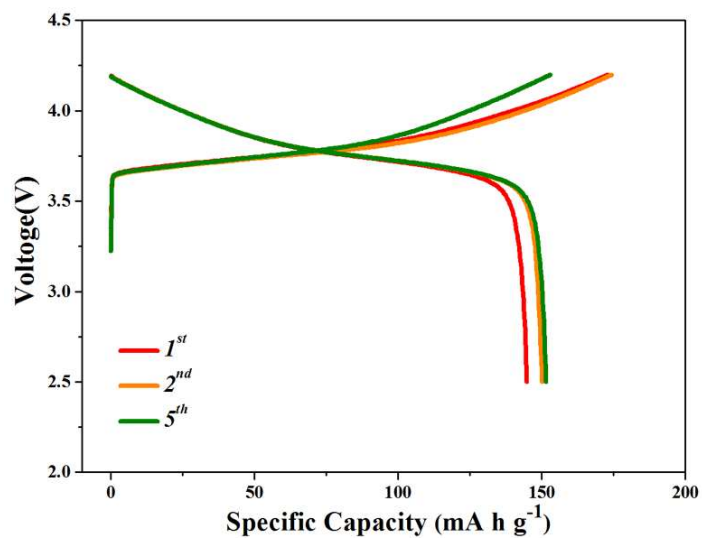


Figure. S11. The typical galvanostatic discharge-charge curves of LNCMO electrode at the current density of 0.5 C (1C=160 mA g⁻¹).

13. Table S2 Comparison of Li-storage performance between HT-NPS@C and previous nickel phosphide structures. (1C = 554 mA g⁻¹)

	Current density	Specific capacity	Cycle number	Ref.
S-Ni₂P@carbon Yolk-shell spheres (HT-NPS@C)	0.4 A g ⁻¹	430 mA h g ⁻¹	500 cycles	This work
Ni₂P@carbon Yolk-shell spheres (NP@C)	0.2 A g ⁻¹	220 mA h g ⁻¹	200 cycles	This work
Ni₂P nanotubes (NTs)	0.5 A g ⁻¹	310 mA h g ⁻¹	100 cycles	Ref ¹
Ni₂P@C nanocomposite	0.1 A g ⁻¹	435 mA h g ⁻¹	50 cycles	Ref ²
Porous Ni₂P nanosheets	0.1 A g ⁻¹	380 mA h g ⁻¹	50 cycles	Ref ³
Ni₂P@C nanoparticles	55.4 mA g ⁻¹	200 mA h g ⁻¹	2 cycles	Ref ⁴
Ni₂P/graphene sheets	55.4 mA g ⁻¹	450 mA h g ⁻¹	50 cycles	Ref ⁵
Peapod-like Ni₁₂P₅@C	100 mA g ⁻¹	660 mA h g ⁻¹	100 cycles	Ref ⁶
Ni₂P nanorods	55.4 mA g ⁻¹	507 mA h g ⁻¹	100 cycles	Ref ⁷
Ni₅P₄/C composite	55.4 mA g ⁻¹	435 mA h g ⁻¹	50 cycles	Ref ⁸

Reference

- Lu, Y.; Tu, J.; Xiong, Q.; Qiao, Y.; Zhang, J.; Gu, C.; Wang, X.; Mao, S. X., Carbon-Decorated Single-Crystalline Ni₂P Nanotubes Derived from Ni Nanowire Templates: A High-Performance Material for Li-Ion Batteries. *Chem.-Eur. J* **2012**, *18*, 6031-6038.
- Lu, Y.; Tu, J.-p.; Gu, C.-d.; Wang, X.-l.; Mao, S. X., In Situ Growth and Electrochemical Characterization Versus Lithium of a Core/Shell-Structured Ni₂P@C Nanocomposite Synthesized by a Facile Organic-Phase Strategy. *J. Mater. Chem.* **2011**, *21*, 17988-17997.
- Lu, Y.; Tu, J.-p.; Xiong, Q.-q.; Zhang, H.; Gu, C.-d.; Wang, X.-l.; Mao, S. X., Large-Scale Synthesis of Porous Ni₂P Nanosheets for Lithium Secondary Batteries. *CrystEngComm* **2012**, *14*, 8633-8641.
- Carenco, S.; Surcin, C.; Morcrette, M.; Larcher, D.; Mézailles, N.; Boissière, C.; Sanchez, C., Improving the Li-Electrochemical Properties of Monodisperse Ni₂P Nanoparticles by Self-Generated Carbon Coating. *Chem. Mat.* **2012**, *24*, 688-697.
- Lu, Y.; Tu, J.; Xiang, J.; Wang, X.; Zhang, J.; Mai, Y.; Mao, S., Improved Electrochemical Performance of Self-Assembled Hierarchical Nanostructured Nickel Phosphide as a Negative Electrode for Lithium Ion Batteries. *J. Phys. Chem. C* **2011**, *115*, 23760-23767.
- Zhang, H.; Feng, Y.; Zhang, Y.; Fang, L.; Li, W.; Liu, Q.; Wu, K.; Wang, Y.,

Peapod-Like Composite with Nickel Phosphide Nanoparticles Encapsulated in Carbon Fibers as Enhanced Anode for Li-Ion Batteries. *ChemSusChem* **2014**, *7*, 2000-2006.

7. Li, Q.; Ma, J.; Wang, H.; Yang, X.; Yuan, R.; Chai, Y., Interconnected Ni₂P Nanorods Grown on Nickel Foam for Binder Free Lithium Ion Batteries. *Electrochim. Acta* **2016**, *213*, 201-206.

8. Lu, Y.; Tu, J. P.; Xiong, Q. Q.; Xiang, J. Y.; Mai, Y. J.; Zhang, J.; Qiao, Y. Q.; Wang, X. L.; Gu, C. D.; Mao, S. X., Controllable Synthesis of a Monophase Nickel Phosphide/Carbon (Ni₅P₄/C) Composite Electrode Via Wet-Chemistry and a Solid-State Reaction for the Anode in Lithium Secondary Batteries. *Adv. Funct. Mater.* **2012**, *22*, 3927-3935.